Electronic Supplementary Material (ESI) for RSC Advances.

Correlating the Magnetism and Gas Sensing Properties of Mn-Doped ZnO Films Enhanced by UV Irradiation

David E. Motaung[1,*], Ioannis Kortidis[3], Gugu H. Mhlongo[1], Mart-Mari Duvenhage[2], Hendrik C. Swart[2], George. Kiriakidis[3], Suprakas Sinha Ray[1]

[1]DST/CSIR National Centre for Nano-Structured Materials, Council for Scientific and Industrial Research, Pretoria 0001, South Africa

[2]Department of Physics, University of the Free State, P.O. Box 339, Bloemfontein ZA9300, South Africa

[3]Institute of Electronic Structure and Laser, Foundation for Research and Technology, Hellas, Heraklion 71110, Crete, Greece

SUPPLEMETARY INFORMATION:

Vibrating sample magnetometer measurements

The magnetization (*M-H)* measurements of the Mn-ZnO films were extracted at room temperature using a Lakeshore 735 vibrating sample magnetometer (VSM) and a sample holder of high-purity Perspex free from any metallic impurity. A special care was taken during the measurements to avoid any trace magnetic contamination **[1, 2]**. Prior the analyses, the sample holder was ultrasonically cleaned to avoid any magnetic contamination. Additionally, the same measurement procedure was repeated for the empty sample holder and a small magnetic signal generated by the sample holder was subtracted from the measured magnetization data of the samples.

*Corresponding Author: Dr. David Motaung, Tel: (+27) 12 841 4775,
Fax: (+27) 12 841 2229, Email: dmotaung@csir.co.za

Results and Discussion

It is well known that XPS is a useful technique to monitor the various behaviours of point defects, such as vacancies and interstitials. Therefore, XPS measurements were carried out to investigate the intrinsic defects in Mn-ZnO films. Fig. S1 shows the typical XPS wide survey spectra of undoped and Mn-doped ZnO films. Three main elements (i.e., O, Zn, and Mn) were observed in the survey scan of the XPS spectra. The detected carbon peak corresponds to the carbon adsorbed on the surface during exposure of the sample to the ambient atmosphere. The binding energies of all the spectra were calibrated by the adventitious carbon C1s peak (~284.6 eV).

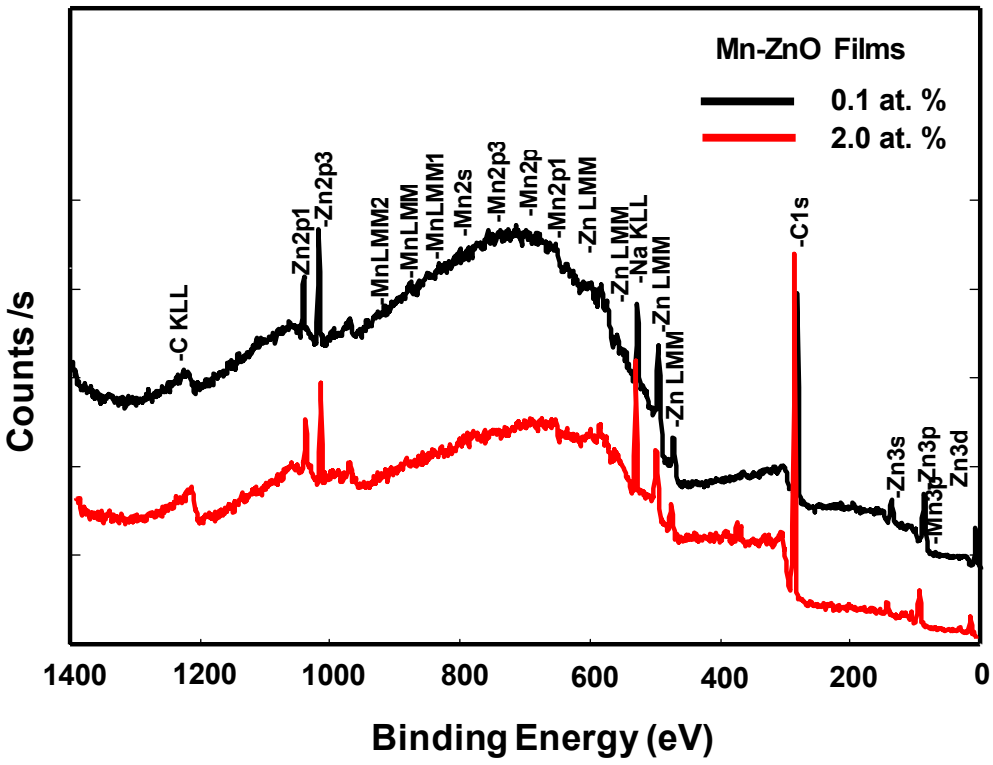

Fig. S1: XPS survey scan of the Mn-doped ZnO films.

Fig. S2 presents the 3D TOF-SIMS micrographs for Zn and Mn layers. The micrograph in Fig. S2b shows that the Mn is not uniformly distributed; it only segregated almost at the edge of the substrate. Moreover, from the overlay image in Fig. S2d, it appears that some of the Mn-ZnO penetrated the Si substrate.

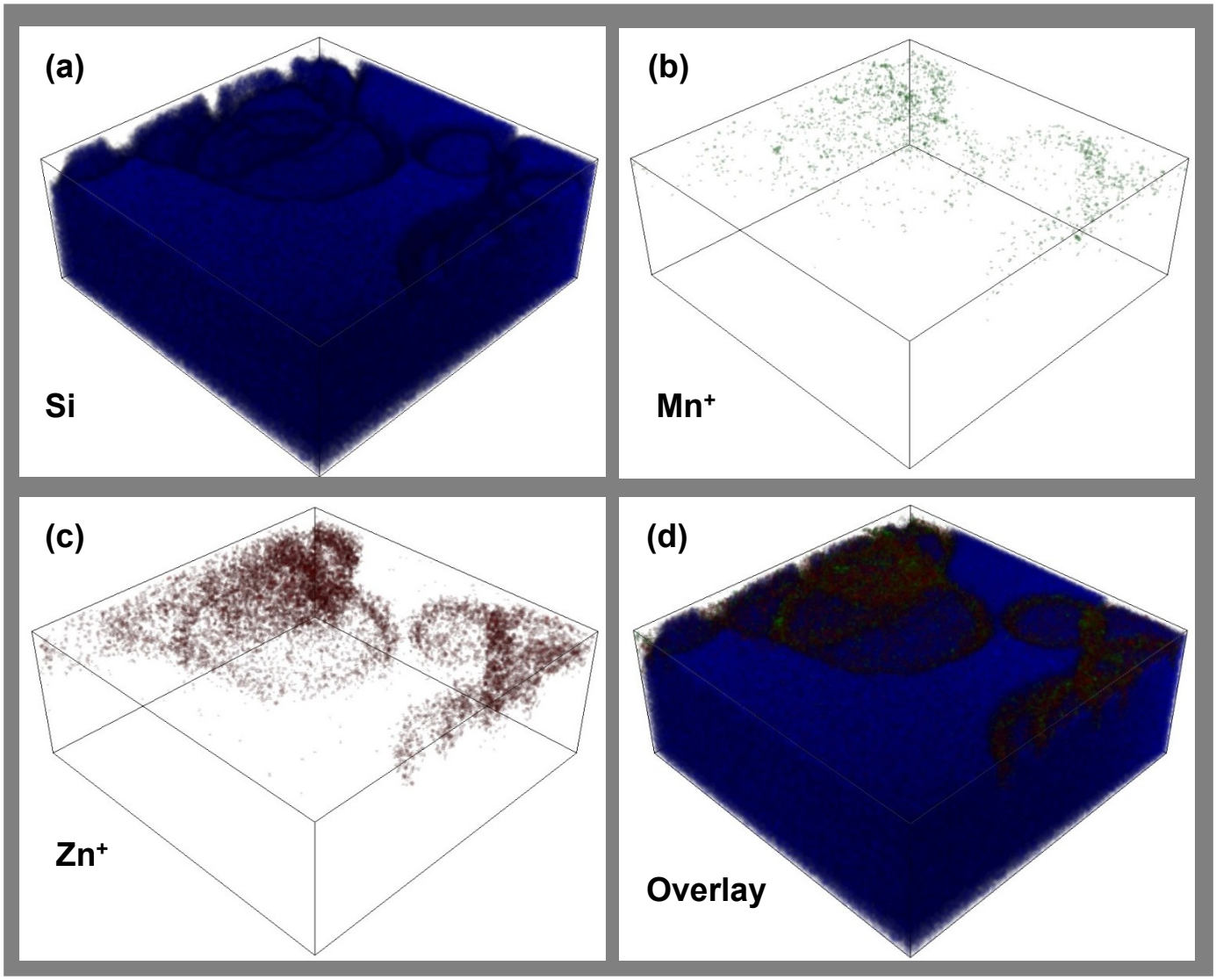

Fig. S2: 3D cross-section TOF-SIMS images for (a) Si substrate, (b) Mn^+, (c) Zn^+ and (d) an overlay of the micrographs.

Fig. S3 shows the 2D overlays of Si^+, Mn^+ and Zn^+ after 2 seconds (a), 25 seconds (b) and 150 seconds of 1.0 at. % Mn-ZnO. In Fig. S3(a) it can be seen that the whole area is not covered by Zn^+ and Mn^+. The Si^+ is clearly visible on the surface of the sample and from the profile it appears that the Si and ZnO are interdiffused. This is however due to the topographic effect.

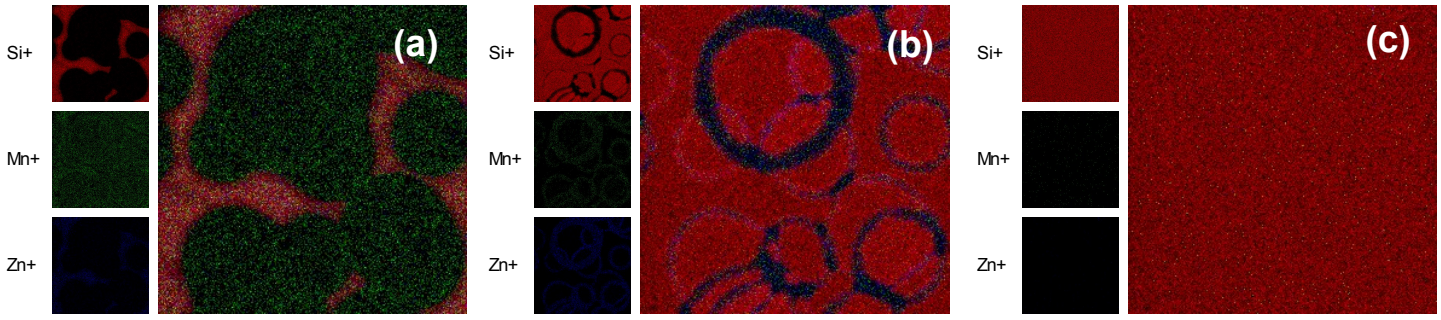

Fig. S3: Overlay images of Si^+ (red), Mn^+ (green) and Zn^+ (blue) after (a) 2 seconds, (b) 25 seconds and (c) 150 seconds. Note these images correspond to 1.0 at. % Mn-ZnO film.

Fig. S4 shows a schematic diagram of the 1.0 at. % Mn-ZnO sample. The red represents the Si (corning substrate) and the blue doughnut (or ring) the ZnO with Mn. From the 3D view (Fig. 4Sa) it can be seen that the ring is on top of the substrate. This is more evident from the side view (Fig. 4Sb), but from the top view (Fig. 4Sc) it seems as if the doughnut and substrate are on the same level. The TOF-SIMS is unable to distinguish between height differences and therefor it seems from the profile that the Si and ZnO are interdiffused.

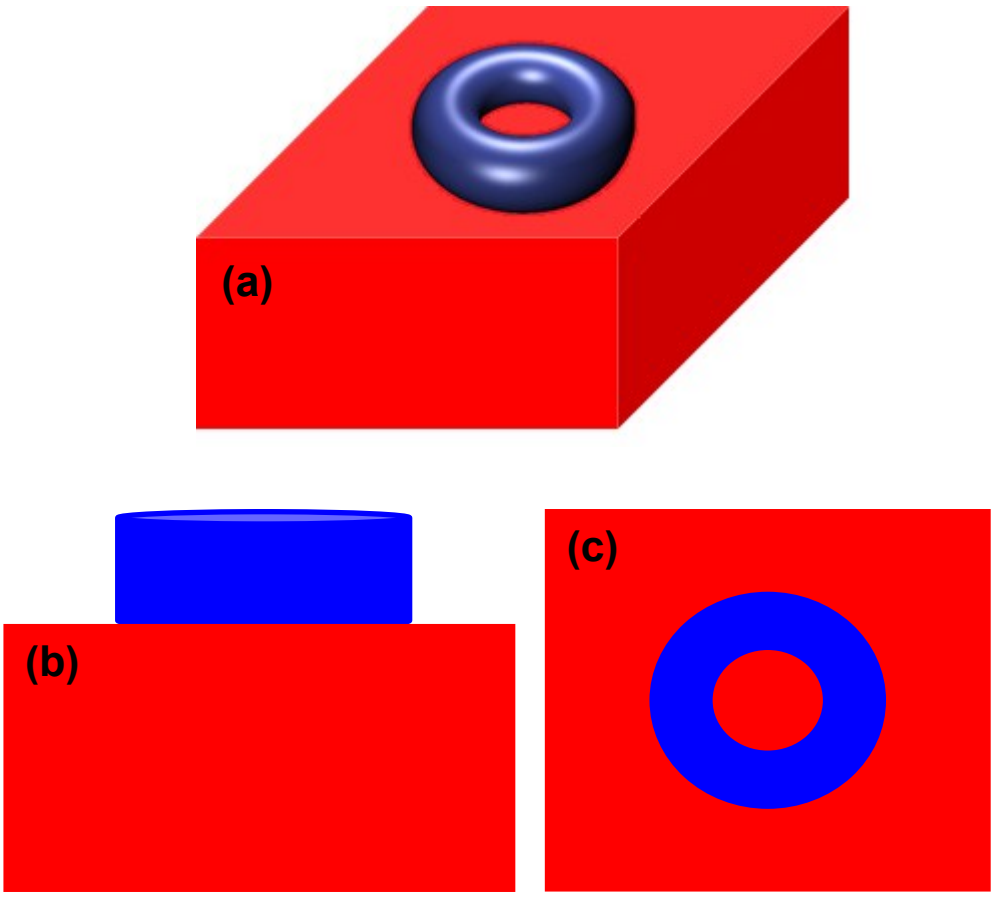

Fig. S4: Schematic diagram of the ZnO (blue) sample on a glass substrate (red). (a) 3D view, (b) side view and (c) top view.

The topographic effect can be minimized by taking the depth profile on selected parts of the 2D image using the analysis software measurement explorer. Fig. S5(a) shows the secondary ion image of the 1.0 at % film. The blue regions represent the Si^+ and the green regions the Zn^+ and Mn^+. The corresponding profiles in Fig. S5 (b) and (c) are different from each other (as well as from Fig. S2). In Fig. S5b there is only a small amount of Zn^+ and Mn^+ on the surface, most probably due to surface contamination and the intensity of the Si^+ increases almost immediately and then becomes stable throughout the profile. This profile represents the glass substrate. In Fig. S5(c), the Zn^+ and Mn^+ intensities increase from the surface and a profile representing the Mn-ZnO doughnut on the surface are present. The Si^+

intensity also rises almost from the surface. It is clear that the doughnuts are quite thin, since that within 10 seconds of sputter the substrate starts getting exposed. Fig. S5(c) shows a better representation of the sputter time profile than in Fig. S3.

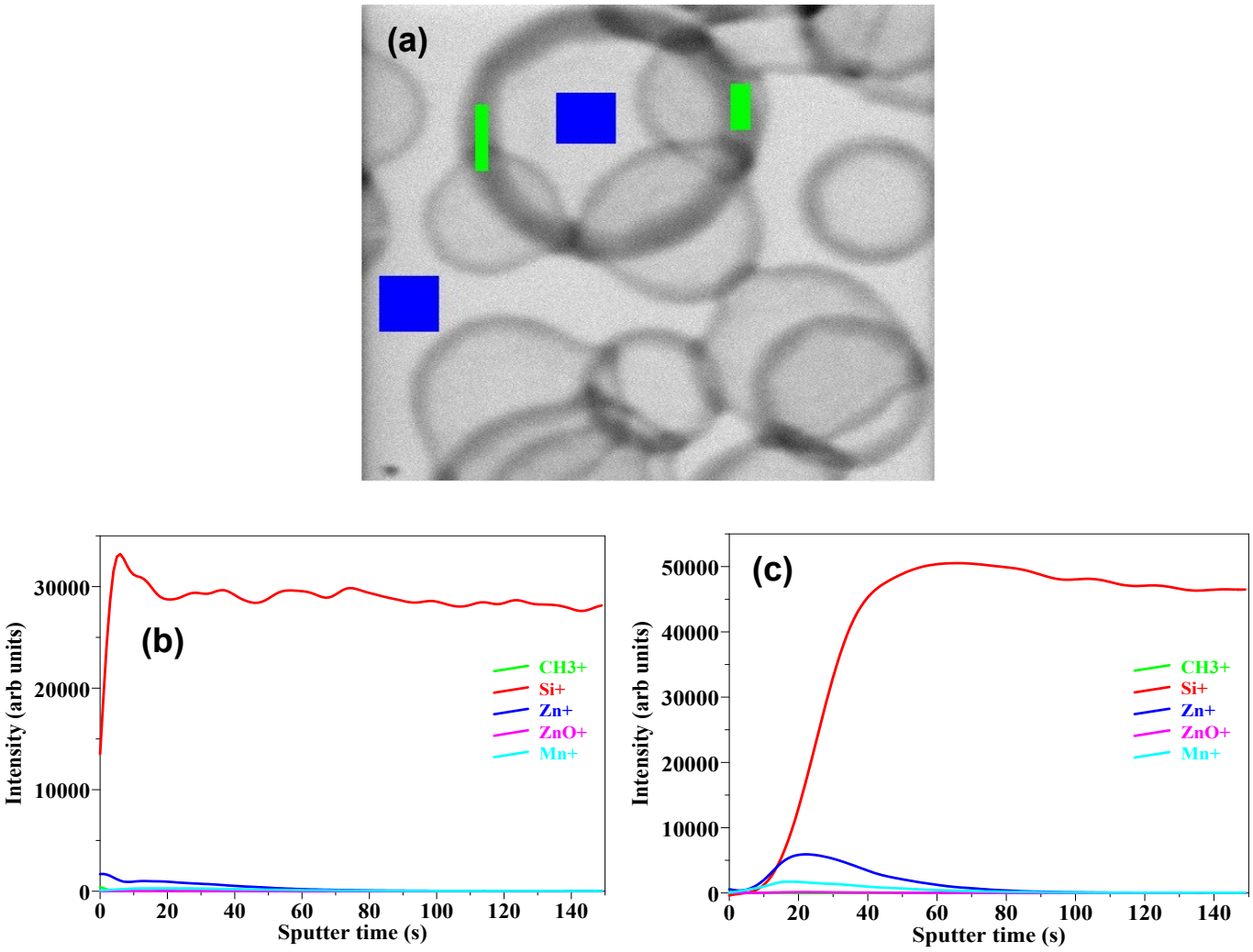

Fig. S5: (a) Secondary ion image of the 1.0 at.% Mn-ZnO sample. Sputter time profile of the blue parts (b) and green parts (c).

Fig. S6 shows the spectra of Si^+ (a), Mn^+ (b) and Zn^+ (c) of the of the 1.0 at.% Mn-ZnO sample. It can be seen that the intensity of the Si^+ peak increases with sputter time. This corresponds to more of the substrate being exposed with sputter time. There is only a small amount of Mn^+ present on the surface of the sample. It

increases after 25 seconds, showing that the Mn^+ is inside the ZnO doughnut. There is Zn^+ on the surface of the sample and the intensity increases after 25 seconds. This confirms the presence of the ZnO doughnut. Very little Mn^+ and Zn^+ are present after 150 seconds. This indicated that the doughnuts were completely sputtered away and only the glass substrate was left.

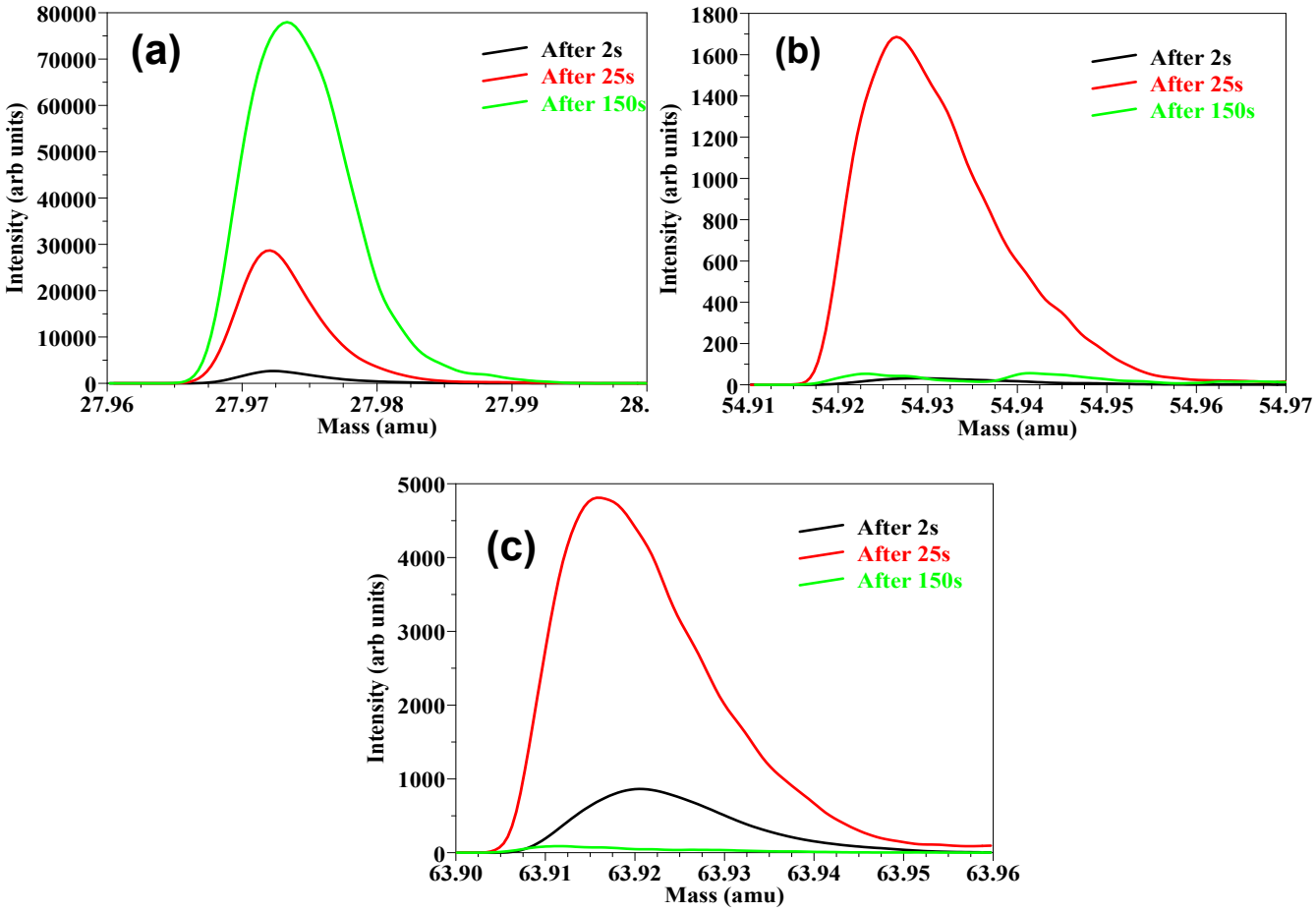

Fig. S6: (a) Si^+, (b) Mn^+ and (c) Zn^+ peak intensities after 2 seconds, 25 seconds and 150 seconds.

The results in Fig. S7 are quite similar to that of Fig. S5, although for the 2.0 at.% Mn ZnO sample. In Fig. S7 (b), it can be seen that at shorter sputtering time the Si^+ intensity increases and then stabilize at longer sputtering time. There is again a small amount of Mn^+ and Zn^+ present on the surface. Fig. S7(c) represents the

spectrum sputtered at the doughnut containing ZnO and Mn. It is observed from the spectrum that the Si^+ intensity only reach its maximum when the doughnut is completely sputtered away.

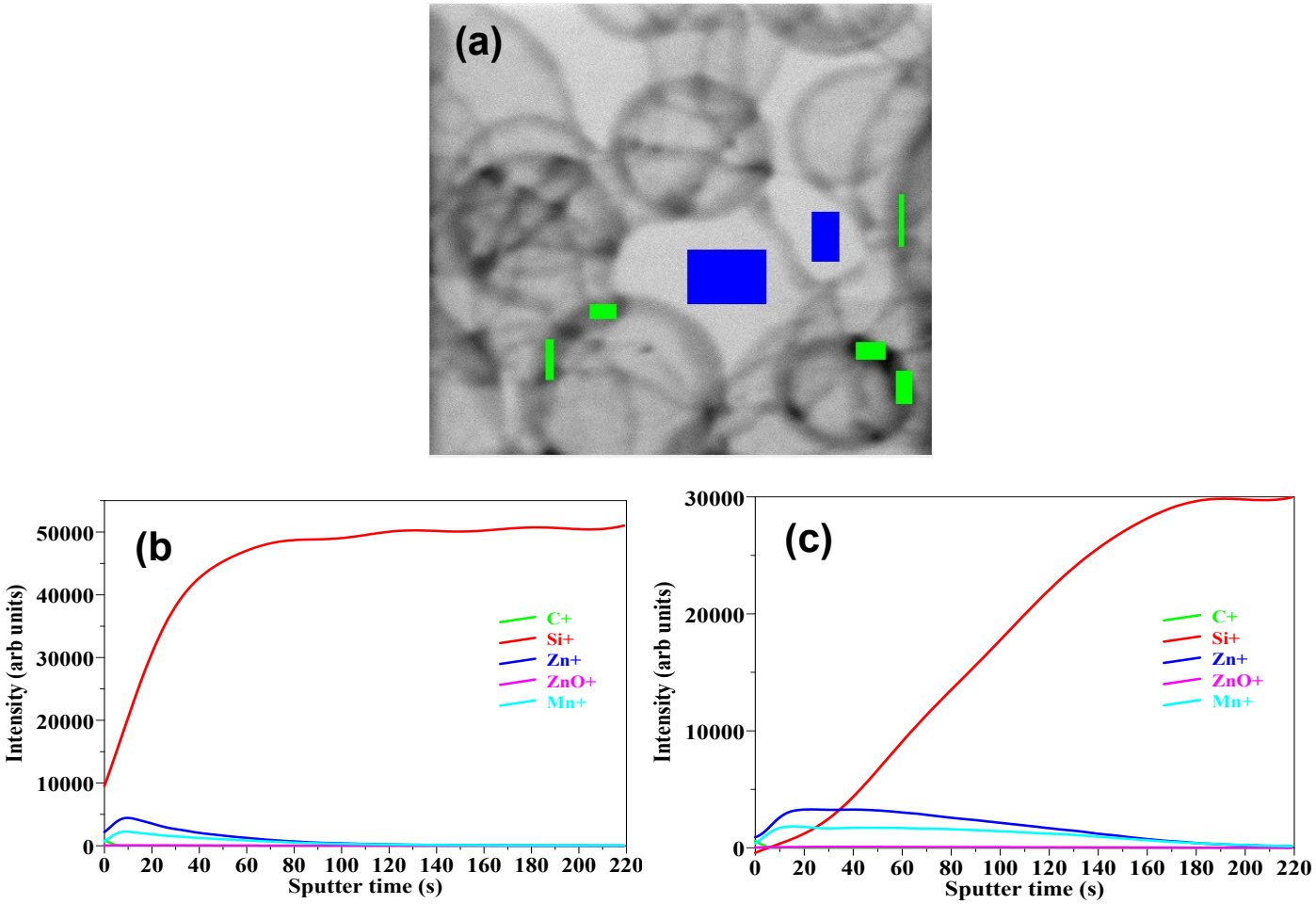

Fig. S7: (a) Secondary ion image of the 2.0 at.% Mn-ZnO sample. Sputter time profile of the blue parts (b) and green parts (c).

Fig. S8 presents SIMS depth profile results of Mn-doped ZnO films grown using ASP. The relative sensitivity factors (RSF) of ZnO^+ and Mn^+ were much lower than those of Si^+ and Zn^+ **[1]**. The intensity of ZnO^+ and Mn^+ was multiplied by 10 for clarity. For all the samples, CH_3^+ was only present on the surface, and it immediately disappeared after the first 5 s of sputtering. The presence of Mn^+ is clearly visible in

the spectra. It can also be concluded that the Mn^{+} occupied the same position as the ZnO^{+} as it followed the same profile. Vinod et al. **[2]** reported that some of the Mn ions probably diffuse substitutionally into the ZnO lattice, substitute for the Zn ions and introduce more defects and lattice distortions, since the ionic radius of Mn^{2+} is larger than that of Zn^{2+}. According to the profiles, it appears that Si and Zn interdiffused. However, this is a topographic effect (for more details, see the Supplementary Information) **[3]**.

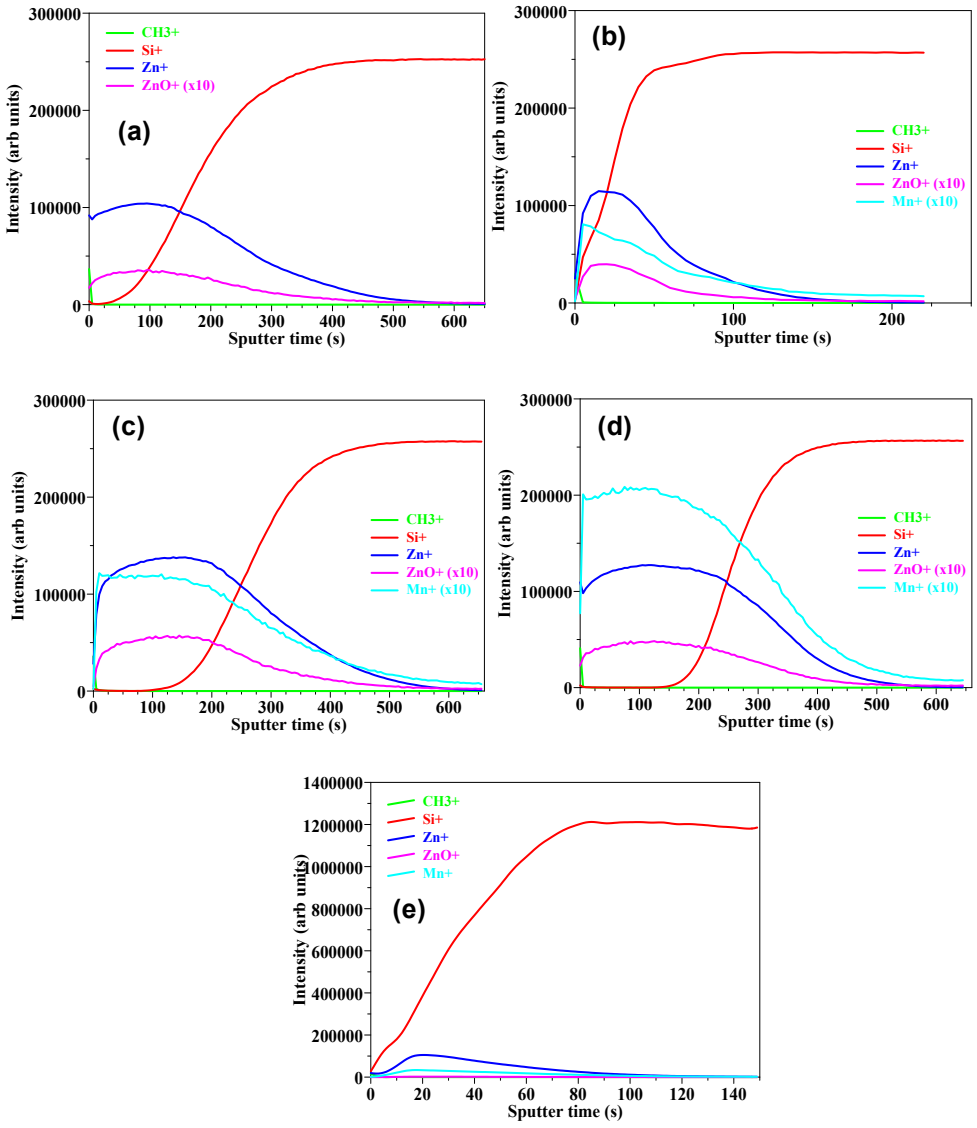

Fig. S8: SIMS depth profile of (a) pure ZnO (b) 0.1 at. %, (c) 0.25 at. %, (d) 0.5 at. % and (e) 1.0 at. % Mn-ZnO films grown using ASP.

Fig. S9 shows the optical constants, refractive index (n), and extinction coefficient (absorption index) (k) as a function of the Mn concentration. Based on the results in Fig. S9a, n decreased as the Mn concentration increased in the ZnO matrix, which indicates that the amount of refracted light decreased with an increase in Mn dopant, demonstrating that incorporation of Mn induces the films to absorb more light. Since n is an important parameter that reflects not only the optical quality but also the crystallinity of ZnO films, the decrease in n as the Mn concentration increased indicates that the crystalline quality of the films also deteriorated, which was evidenced by the XRD analysis (Fig. 3). This change in n with Mn doping can be explained based on the contribution from both lattice contraction and disorder in the ZnO structure because n values are related to the packing density of the film. Previous studies indicated that low values of n are typically associated with a low film density **[4-6]**. Therefore, based on the above analysis, we can conclude that the refractive index of Mn-doped ZnO thin films primarily depends on the grain size, density, and Mn concentration in the thin films. Fig. S9b shows that, the value of k increased with increasing Mn doping in the ZnO host over a wavelength range of 360-365 nm. This increase in k was primarily due to the observed decrease in the crystallinity of the material, which was confirmed by the XRD analysis (Fig. 3). In addition, k was red-shifted for Mn doping up to 0.25 at. %. This red shift may be due to a reduced quantum confinement effect, and it is consistent with the results reported by Shinde *et al.* **[7], who** attributed it to the fact that absorption of higher energy photons caused activation of ‘spd’ exchange interactions and typical ‘dd’ transitions, which led to the enhancement of ferromagnetic properties. Therefore, we propose that the magnetic properties, especially the room temperature ferromagnetism, may be enhanced with doping between 0.1 and 0.5 at. %.

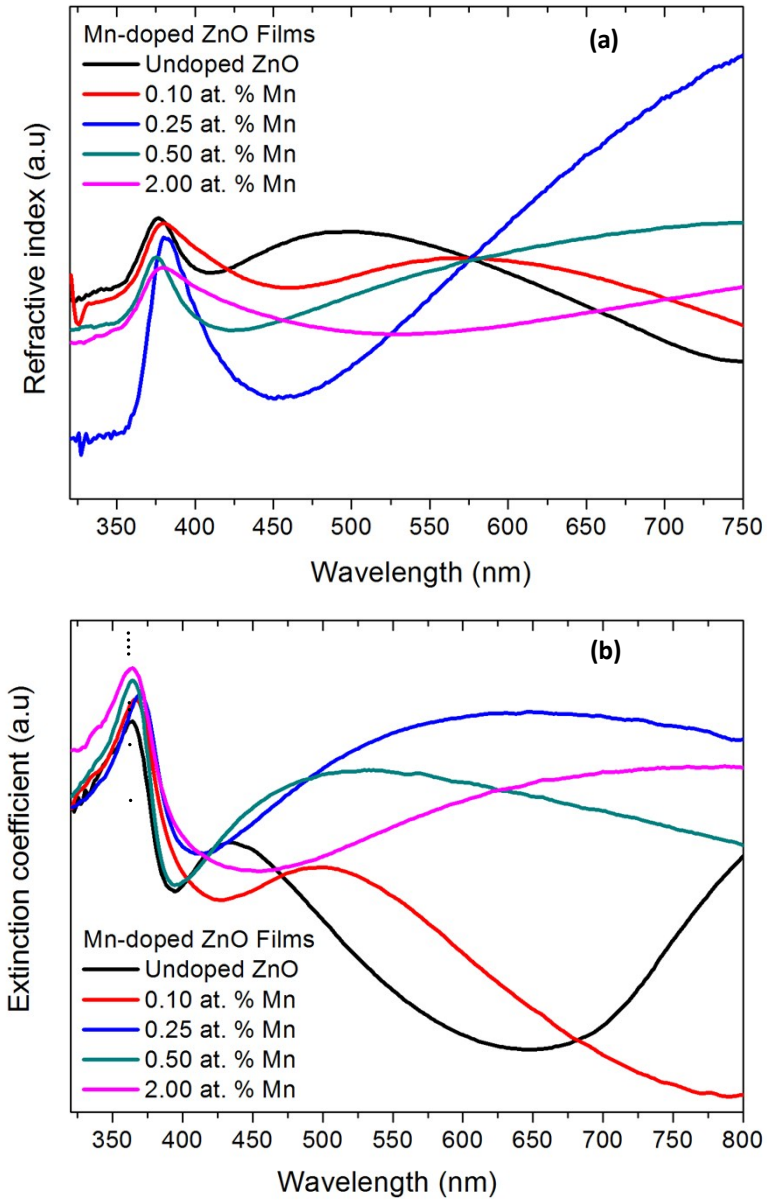

Fig. S9: Evolution of the (a) refractive index (n) and (b) extinction coefficient (k) as a function of the Mn concentration.

Fig. S10 shows the UV-vis absorbance spectra of undoped and Mn-doped ZnO thin films. As shown in Fig. S10a, as dopant concentration increases from 0.1 at.% to 2.0 at.%, the absorbance increases gradually. Fig. S10b shows the optical

band gap estimated using Tauc's plot by extrapolating the linear region of $(\alpha hv)^2$ versus incident photon energy (hv), where α is the absorption coefficient.

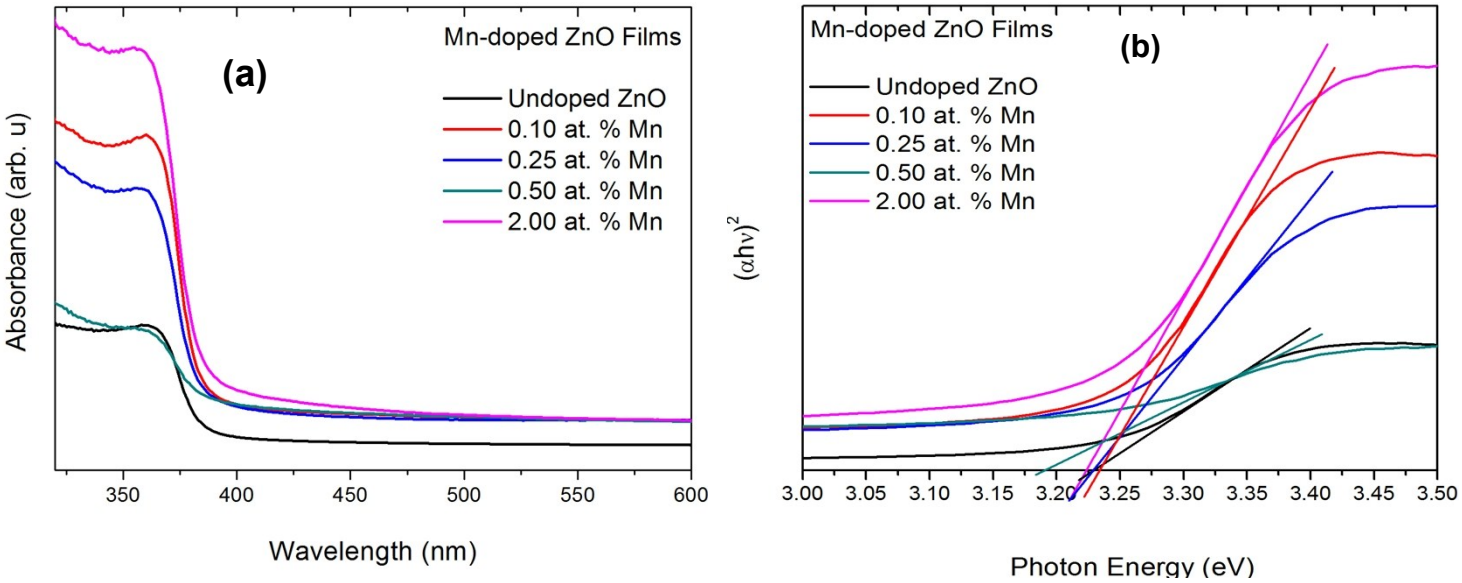

Fig. S10: (a) UV-vis absorbance spectra of Mn doped ZnO films and (b) Tauc's plot.

In order to investigate the magnetic property of Mn-ZnO films, magnetization measurement was performed using vibrating sample magnetometer. The recorded *M–H* data had been subtracted from the diamagnetic contribution arising from the background signal of the substrate. As shown in Fig. S11a, the material contains features of ferromagnetic (FM) and also small features of paramagnetic are observed. Upon doping the sample with 0.1 at. % Mn (Fig. S11b), a clear hysteresis loop is observed denoting that the film is FM. It is interesting to note that no trace of any Mn and/or Mn oxide cluster were observed in Mn-ZnO doped at lower doping level, as indicated from XRD and TOF-SIMS measurements. Therefore, the observed room temperature FM for the 0.1 at. % Mn-ZnO sample appears to be intrinsic. At higher doping level (2.0 at. % Mn), the FM behaviour is suppressed and paramagnetic nature is enhanced probably due to segregation of Mn as depicted in

TOF-SIMS analyses. The coercive fields of 201.47, 260.85 and 158.04 Oe was observed for the undoped, 0.1 and 2.0 at Mn doped ZnO films respectively.

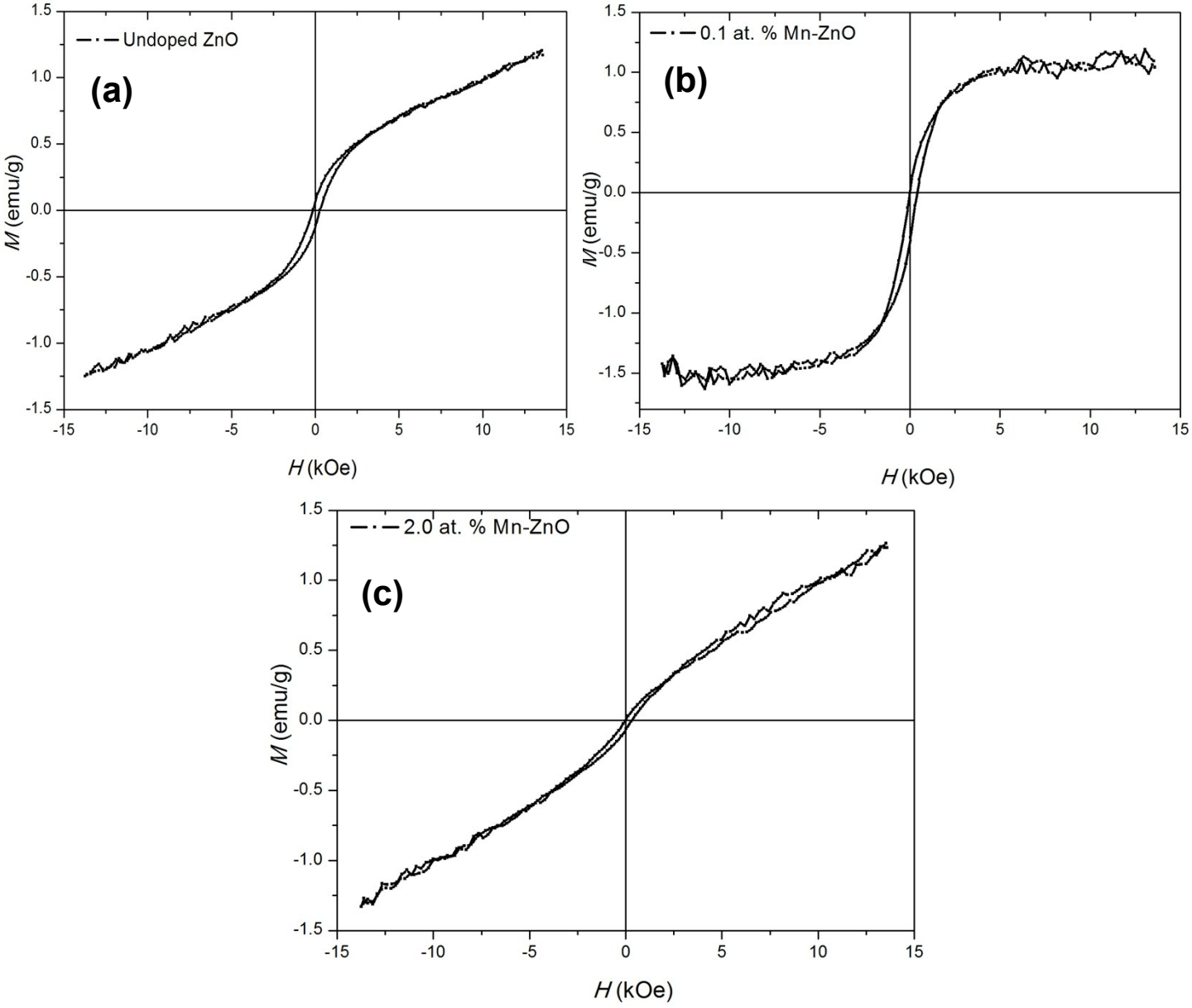

Fig. S11: Room temperature *M-H* curves of (a) Undoped ZnO, (b) 0.1. at. % Mn-ZnO and (b) 2.0 at.% Mn-ZnO films.

Fig. S12 shows the gas sensing response of the 0.1 at. % tested to H_2. As depicted in Fig. S12, the 0.1 at. % sensing does not show a good recovery when tested to H_2 gas compared to CO_2 and NO.

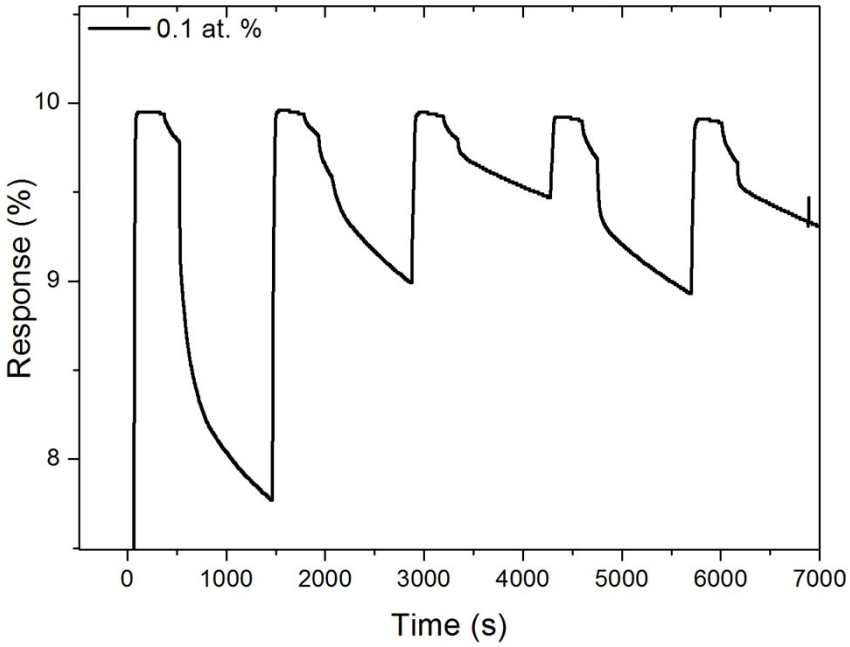

Fig. S12: Sensing performance and repeatability of 0.1 at. %Mn-ZnO sensing film exposed to H_2 gas at room temperature over a long working period.

References

[1] M.A. García, E.F. Pinel, J. de la Venta, A. Quesada, V. Bouzas, J.L. Fernández, J.L. Romero, M.S. Martn-González, J.L. Costa-Krämer, *J. Appl. Phys*. 2009, **105**, 013925 - 013925-7

[2] D.E. Motaung, G.H. Mhlongo, S.S. Nkosi, G.F. Malgas, B.W. Mwakikunga, E. Coetsee, H.C. Swart, H.M.I. Abdallah, T. Moyo, S.S. Ray, ACS Appl. Mater. Interfaces 2014*,* **6,** 68981-8995

[3] F.A. Stevie, R.G. Wilson, *J. Vac. Sci. Technol*. 1991, **A9***,* 3064-3070.

[4] R. Vinod, M. Junaid Bushiria, S.R. Achary, V. Múnoz-Sanjosé, *Materials Science and Engineering B* 2015, **191**, 1–6.

[5] A. Yousif, R.M. Jafer, J.J. Terblans, O.M. Ntwaeaborwa, M.M. Duvenhage, V. Kumar, H.C. Swart, *Appl. Surf. Sci.* 2014, **313**, 524- 531.

[6] Y. Caglar, S. Ilican, M. Caglar, F. Yakuphanoglu, *Spectrochim. Acta*, Part A 2007, **67**, 1113-1119.

[6] J.P. Zhang, G. He, L.Q. Zhu, M. Liu, S.S. Pan, L.D. Zhang, *Appl. Surf. Sci.* 2007, **253**, 9414-9421.

[7] E. Cetinorgu, S. Goldsmith, V.N. Zhitomirsky, R.L. Boxman, C.L. Bungay, *Semicond. Sci. Technol.* 2006, **21**, 1303-1310.

[8] V.R. Shinde, T.P. Gujar, C.D. Lokhande, R.S. Mane, S.-H. Han, *Mater. Chem. Phys*. 2006, **96**, 326-330.